Flow Turbulence Combust (2013) 90:95–119
DOI 10.1007/s10494-012-9429-5

Near Field Round Jet Flow Downstream from an Abrupt Contraction Nozzle with Tube Extension

X. Grandchamp · A. Van Hirtum

Received: 5 April 2012 / Accepted: 2 November 2012 / Published online: 14 December 2012

Abstract Round air jet development downstream from an abrupt contraction coupled to a uniform circular tube extension with length to diameter ratio $L/D = 1.2$ and $L/D = 53.2$ is studied experimentally. Smoke visualisation and systematic hot film velocity measurements are performed for low to moderate Reynolds numbers $1130 < Re_b < 11320$. Mean and turbulent velocity profiles are quantified at the tube exit and along the centerline from the tube exit down to 20 times the diameter D. Flow development is seen to be determined by the underlying jet structure at the tube exit which depends on Reynolds number, initial velocity statistics at the tube exit and the presence/absence of coherent structures. It is shown that the tube extension ratio L/D as well as the sharp edged abrupt contraction influence the initial jet structure at the tube exit. For both L/D ratios, the presence of the abrupt contraction results in transitional jet flow in the range $2000 < Re_b < 4000$ and in flow features associated with forced jets and high Reynolds numbers $Re_b > 10^4$. The tube extension ratio L/D downstream from the abrupt contraction determines the shear layer roll up so that for $L/D = 1.2$ flow visualisation suggests the occurrence of toroidal vortices for $Re_b < 4000$ whereas helical vortices are associated with the transitional regime for $L/D = 53.2$. Found flow features are compared to features reported in literature for smooth contraction nozzles and long pipe flow.

Keywords Axisymmetrical jet · Anemometry · Initial conditions · Jet forcing · Moderate Reynolds numbers · Transition regime · Vortex dynamics

X. Grandchamp · A. Van Hirtum (✉)
GIPSA-lab, UMR CNRS 5216,
Grenoble University, Grenoble, France
e-mail: annemie.vanhirtum@gipsa-lab.grenoble-inp.fr

1 Introduction

Due to numerous experimental and numerical studies of round free jet flows, an overall good knowledge and understanding of these flows exist for long pipes and smooth contraction nozzles. The time averaged turbulent jet flow mixing region is schematically divided into three parts: an initial near field region downstream the exit, a transition region and a self-preserving far field region further downstream. In this third zone, the axisymmetric jet flow is typically modelled by a simple decay equation [39]:

$$\overline{U}_c(x) = \frac{\overline{U}_0 K D}{x - x_0}, \tag{1}$$

where $\overline{U}_c$ denotes the mean centerline velocity in the axial direction x, $\overline{U}_0$ the centerline mean velocity at the tube exit, K the mean centerline velocity decay coefficient and x_0 the virtual origin. Despite the described universal behaviour it is shown analytically [12] that the velocity decay, and so the decay parameters K and x_0, depends on Reynolds number as well as on initial conditions at the exit of the emitting geometry: exit Reynolds number [33, 35], mean velocity profile at the tube exit [11, 41], turbulence intensity [5, 32, 36, 41], nozzle exit geometry [20, 25, 26, 34], boundary layer thickness [4, 9, 18, 27, 36, 45] and density ratio of the jet fluid to ambient fluid [38].

These former investigations were essentially conducted for high bulk Reynolds number flow, typically 10^4 or higher. Studies dealing with round airflow jets for low and moderate bulk Reynolds number, $Re_b < 10^4$, are few and mostly deal with the influence of Reynolds number on jet development along the centerline expressed by decay coefficient K, virtual origin x_0 and potential core extent x_{pc} [2, 21, 24, 33]. In general, it is observed that for decreasing Reynolds number the velocity decay fastens [2, 21, 24, 33]. As a result the potential core extent gets shorter [2, 24, 33], although the opposite is reported in [21] where for decreasing Reynolds number in the range $177 \leq Re_b \leq 5142$ [21], the potential core extent increases.

Besides the velocity decay of the round airflow jet in the self-preserving region, the influence of initial conditions at the nozzle exit on the formation and development of coherent structures in the near field of round jet airflow is shown experimentally for low [23, 40] as well as high [5, 9, 34, 45] Reynolds numbers. Therefore experimental results confirm the severe influence of the initial shear layer momentum thickness and initial mean velocity profile predicted theoretically [6, 8, 22, 28, 29].

Due to the influence of initial conditions at the nozzle exit on jet flow development in the near and far field most of the cited studies deal with carefully designed emitting geometries avoiding the transition regime such as smooth contraction nozzles [30, 31] and long pipe nozzles with length to diameter ratio $L/D > 40$ [43, 44]. Nevertheless, the emitting geometries and flow facilities vary considerably with respect to size, grid use, nozzle contraction ratio, length to diameter ratio and wall thickness at the outlet which are all known to affect initial conditions. Therefore, even in case standarised nozzles are used, flow development can be altered by differences in the flow facility. In order to increase insight in the effect of the emitting geometry on jet development it is favourable to study different geometries using the same flow facility.

Round jet airflow development downstream from a smooth contraction nozzle, sharp-edged orifice nozzle or long pipe nozzle with $L/D > 40$ are studied in litera-

ture for a single Reynolds number, such as $Re_b = 8.6 \times 10^4$ [45], $Re_b = 1.84 \times 10^5$ [34] and $Re_b = 1.6 \times 10^4$ [27]. A more systematic study for Reynolds numbers in the range $850 \leq Re_b \leq 6750$ for purely laminar exit flow is presented in [40] for a single nozzle flush in a wall. Consequently, systematic studies of jet dynamics with respect to moderate Reynolds numbers, $Re_b < 10^4$, and emitting geometry are needed.

The current study aims to contribute to the understanding of flow development and generation of coherent structures in the mixing layer of the round jet issuing from a circular uniform pipe downstream from a sharp edged abrupt contraction for low to moderate Reynolds numbers. Initial conditions at the pipe exit are varied by considering two pipe length to diameter ratios L/D and by systematically varying the Reynolds number in the range $10^3 < Re_b < 1.2 \times 10^4$. The abrupt contraction is characterised by a large area contraction ratio as the contraction ratio used by [23]. The length of the short pipe nozzle is chosen so that the length to diameter ratio yields $L/D = 1.2$ which is similar as the length to diameter ratio of the contraction nozzle used in [23] and exceeds the L/D ratio characterising an orifice nozzle. The initial mean velocity profile is expected to be characterised by a constant velocity in a large core center region based on data presented in [23, 30, 31]. As a reference, a long pipe nozzle with length to diameter ratio $L/D > 40$, $L/D = 53.2$, is studied using the same flow facility. For a long pipe nozzle a constant velocity portion in the mean profile at the exit is expected to be absent [27, 45]. Consequently, the influence of an abrupt contraction on the initial conditions at the nozzle exit and flow development is studied experimentally as function of Reynolds number for $L/D = 1.2$ and $L/D = 53.2$. Obtained results are compared to results for smooth contraction nozzles and long pipe nozzles reported in literature. Radial velocity distributions at the tube's exit and axial velocity distributions along the jet centerline are quantified by hot film anemometry. In addition, smoke visualisation is performed. The generation of coherent structures in the near field downstream the tube exit is discussed.

An extended abrupt contraction nozzle is simple to manufacture and might therefore provide a simple flow control device in technological jet applications in case its development can be characterised. In addition, increased understanding of the flow issuing from such nozzles contributes to biofluids mechanics where sharp edges and moderate Reynolds numbers occur naturally.

2 Experimental Setup

2.1 Channel flow facility

The channel flow facility, illustrated in Fig. 1, consists of an air compressor (Atlas Copco GA7), followed by a pressure regulator (Norgren type 11-818-987) providing an airflow at constant pressure. The volume flow rate is controlled by a secondary manual valve placed downstream the regulator and measured by a thermal mass flow meter (model 4043 TSI) with an accuracy of 2 % of its reading. To homogenize the flow, a settling chamber is used with volume $0.25 \times 0.3 \times 0.35$ m^3 to which a series of 3 perforated plates with holes of diameter 0.0015 m are added. The walls of the settling chamber are tapered with acoustic foam (SE50-AL-ML Elastomeres Solutions) in order to avoid acoustic resonances. Downstream the settling chamber, a uniform extension tube of diameter $D = 25$ mm and varying length L is connected with

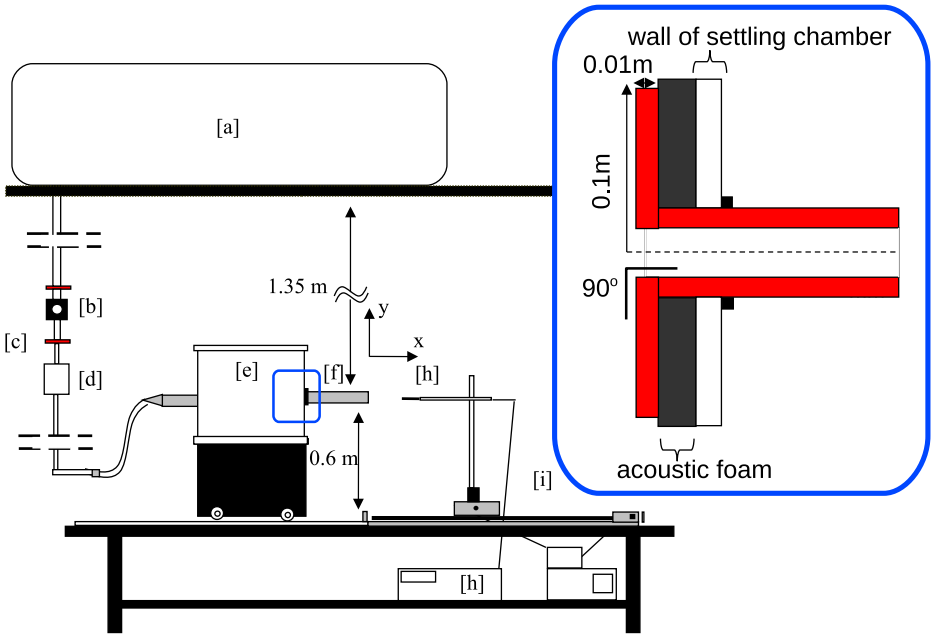

Fig. 1 Sketch of the setup: [a] air compressor, [b] pressure regulator, [c] valve, [d] volume flow rate, [e] settling chamber, [f] pipe section, [g] hot film, [h] IFA-300 TSI and [i] positioning system, [zoom] mounting of the sharp-edged abrupt contraction to the settling chamber

a flat disk to ensure an axisymmetric pipe inlet [13]. Thus the airflow sustains an abrupt area contraction equal to 40:1 from the settling chamber to the pipe. During experiments 2 tube lengths are assessed, $L = 3$ and $L = 133$ cm, corresponding to length-to-diameter ratios $L/D = 1.2$ and $L/D = 53.2$.

The imposed volume airflow rates Q are varied from 20 l/min up to 200 l/min by 10 l/min steps, in order to explore bulk Reynolds numbers in the range $10^3 < Re_b < 1.2 \times 10^4$. The bulk Reynolds number Re_b is defined from pipe bulk velocity U_b and pipe diameter D as $Re_b = \frac{U_b D}{\nu} = \frac{4Q}{\nu \pi D}$ with air kinematic viscosity $\nu = 1.5 \times 10^{-5}$ m^2/s.

For all experiments, the jet airflow velocity is studied with a hot film (model 1201-20 TSI), having a diameter of 50.8 μm and a working length of 1.02 mm, used in combination with a IFA 300 anemometer (TSI). All data are collected on a 16 bit A/D data acquistition chard (National Instruments). The hot film is calibrated according to the technique described in [14] which results in a calibration curve fitted on a fourth order polynomial law. The hot film is mounted on a two dimensional stage positioning system (Chuo precision industrial co. CAT-C, ALS-250-C2P and ALS-115-E1P) with accuracy of 4 μm in the axial x direction and 2 μm in the radial y direction. The initial jet velocity profile at the tube exit is measured along the radial y direction and the axial centerline velocity profile along the x direction. For the initial radial jet velocity profile the hot film is placed downstream, at a distance $x/D \leq 0.04$, from the pipe exit and the applied radial spatial step yields $\Delta y = 10^{-4}$ m in the range $-0.7 < y/D < 0.7$. Axial velocity data along the jet centerline are collected along

Table 1 Lower and upper limit of Helmholtz resonance frequency and first open tube resonance frequency for length-to-diameter ratios $L/D = 1.2$ and $L/D = 53.2$

	$L/D = 1.2$	$L/D = 53.2$
Helmholtz	$>$ 42Hz and $<$ 60Hz	$>$ 6.4Hz and $<$ 9Hz
Open tube	$>$ 4533Hz	$>$ 127Hz

the pipe axis, at $y/D = 0$, from $x/D \leq 0.04$ up to $x/D < 20D$ with a axial spatial step $\Delta x = 10^{-3}$ m.

Except for the air compressor, the jet facility is placed inside a closed room for which the temperature is controlled in order to minimise flow disturbances. It is verified that in absence of an abrupt contraction nozzle no flow disturbance is generated by the used flow facility [13]. The Helmholtz and open tube resonance frequencies associated with length-to-diameter ratios $L/D = 1.2$ and $L/D = 53.2$ are summarized in Table 1. An upper limit of the Helmholtz resonance frequency is estimated by accounting for a 50 % reduction of the given volume of the settling chamber due to the presence of the acoustic foam and perforated plates.

At each measurement position, velocity data are sampled at 40 kHz during 4 s consecutively. Statistical quantities are calculated from instantaneous velocity measurements to which a 10 kHz low pass filter is applied. The local mean velocity $\overline{U}$ and local turbulence intensity T_U,

$$T_U = \frac{\sigma}{\overline{U}} \text{ with } \sigma = \sqrt{\frac{1}{N_{\text{tot}}} \sum_{p=1}^{N_{\text{tot}}} \left(U_p - \overline{U}\right)^2}, \tag{2}$$

are quantified with N_{tot} denoting the total number of samples, velocity root mean square σ and U_p the p$^{\text{th}}$ instantaneous sample. Uncertainties on mean velocity $\overline{U}$ and turbulence intensity T_U are estimated as $<$3 % for $2 < U_p < 10$ m/s and $<$10 % for $0.4 < U_p < 2$ m/s using the characteristic time scales of order of magnitude 10^{-3} s and 10^{-2} s respectively [13, 14].

2.2 Flow visualisation

Flow visualization is obtained by injection of neutrally buoyant white smoke by means of a fog machine (Kool Light, FOG-1200E, 1200W, maximum volume flowrate 300 m^3/min). The effective Schmidt number of the smoke is of order 10^6. Two dimensional illumination is applied with a two-dimensional laser light beam. The laser light sheet is generated by a class IIIb laser light source (Laserglow Technologies, LRS-0532-TFM-00200-10, 234.2 mW, wavelength of 532 nm and with spectral linewidth $<$ 0.1 nm) to which a 10 degree cylindrical lens is added. The resulting laser sheet has a thickness $<$3 mm. To record the illuminated smoke pattern, a color camera (Casio, EXILIM Pro EX-F1, 6.0 million effective pixels and 12X optical zoom) is positioned perpendicular to the laser sheet. The back wall of the test chamber is painted in black to ensure a good contrast with the smoke pattern. Movies are recorded at 300 fps so that the time interval between consecutive images is 0.0033 s which ensures a good freezing of the flow development. The exposure time used to gather each image is constant and does not depend on the assessed Reynolds number.

3 Results and Discussion

A qualitative description of the flow development is given based on typical flow visualization. A quantitative analysis of point velocity measurements is presented.

3.1 Near field flow visualisation

Instantaneous flow visualisation images of the jet flow for 6 Reynolds numbers $Re_b = 1131, 1697, 2263, 2829, 3961, 11317$ and length to tube diameter ratios $L/D = 1.2$ and $L/D = 53.2$ are illustrated in Fig. 2. The view field extends from the tube exit up to $x \leq 5D$ downstream in order to focus on the near field development.

For the long pipe nozzle, $L/D = 53.2$, no coherent structures are observed in the near field for Reynolds numbers $Re_b = \{1131, 1697\}$. The flow pattern is dominated by a large laminar core. A jet flow instability emerges at Reynolds number $Re_b = 2263$ in accordance with the helical nature of laminar pipe flow for $L/D > 40$ [1, 6, 8, 15, 37, 43]. A further increase in Reynolds number amplifies the instabilities and leads to an important decrease of the laminar core extent and the appearance of a turbulent region. Large axisymmetrical coherent vortices are not observed. The onset of instabilities in the range $2000 < Re_b < 3000$ is in accordance with observations of pipe flow issuing from a smooth long pipe nozzle in case a large disturbance is introduced at the inlet [43, 44]. Therefore, the presence of an abrupt contraction at the pipe inlet can be seen as a geometrical disturbance reducing the Reynolds numbers associated with the transition regime compared to transitional Reynolds numbers $Re_b \approx 10^4$ observed for pipe flow in absence of such disturbances [43, 44].

In case of a short nozzle $L/D = 1.2$, images clearly illustrate the dependence of the flow structure on Reynolds number. For the lowest Reynolds number $Re_b = 1131$ an axisymmetric instability of the flow is observed. The vorticity layer immediately downstream the nozzle exit rolls up so that axisymmetric large scale structures are formed surrounding the potential core and engulfing both ambient and pure jet fluid. Large ring vortices with an elliptic form are generated for which the main axis remains parallel to the main flow direction. The vortical structures persist down to approximately $3D$ before reaching the centerline. Consequently, the interaction of large scale structures and their deformation in the near field is limited so that the centerline velocity at the tube outlet is expected to be only weakly imprinted by the vortex presence. Although a difference in the geometrical configuration compared with [1, 46] where the jet flow exit from a smooth contraction nozzle at Reynolds number $Re_b = 1031$ and $Re_b = 1600$ respectively, the current jet flow remains unstable and this instability is still a Kelvin-Helmholtz instability with an axisymmetric mode. Nevertheless, the presence of the abrupt contraction triggers the shear layer roll up at the nozzle exit so that generation of ring vortices is shifted upstream compared to a smooth contraction nozzle [40].

For $Re_b = \{1697, 2263, 2829\}$ a smaller tailing vortex is observed immediately behind a large leading vortex at $x/D \approx 1$. The collapse of the two vortices into a single one at $x/D \approx 2$ suggests a vortex pairing process to take place at a spatial position observed for transitional jet flow at high Reynolds numbers $Re_b > 10^4$ as described by the two ring model for the axisymmetric jet issuing from a smooth contraction nozzle [15]. This fusion has for consequence to impulse a deformation

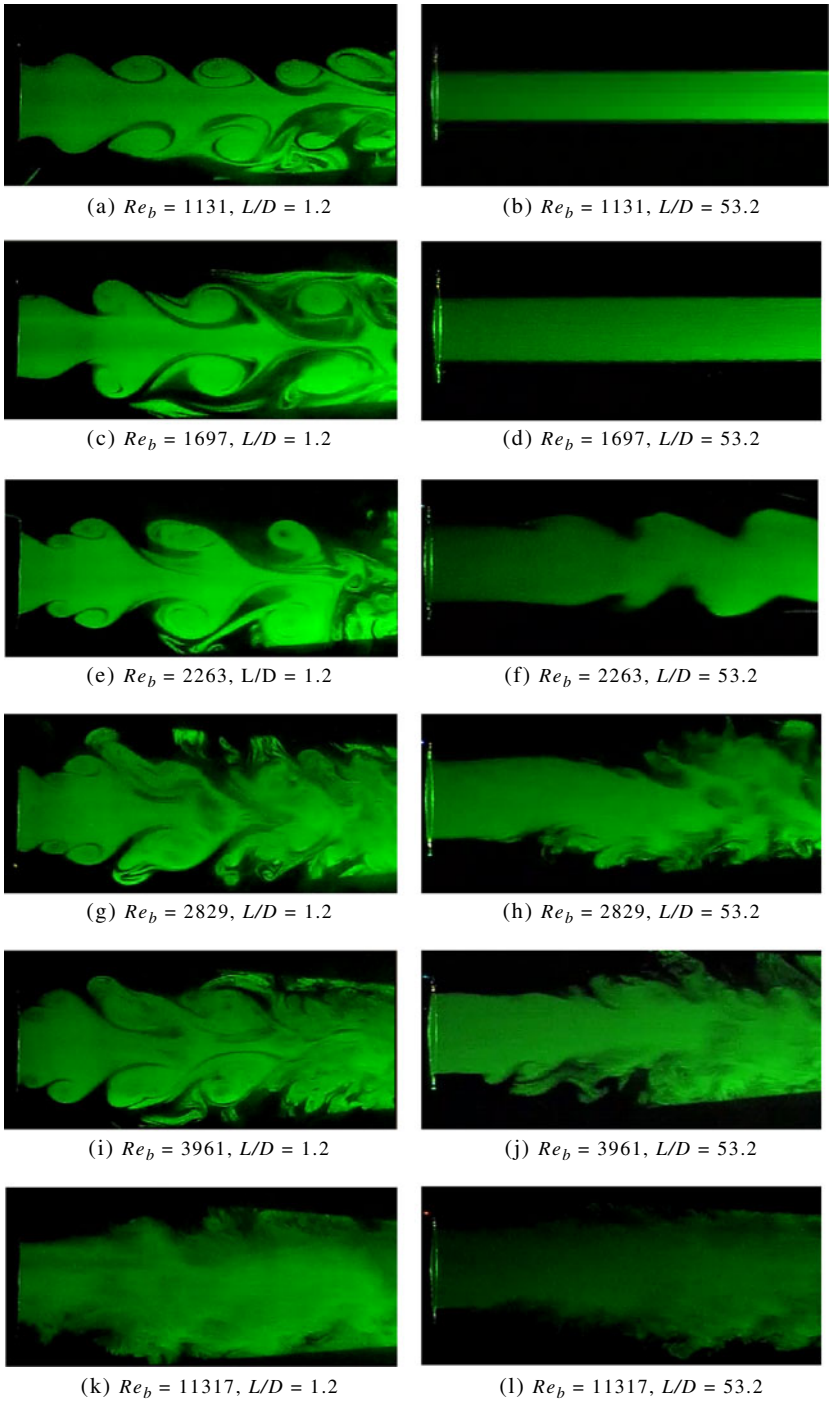

(a) Re_b = 1131, L/D = 1.2 (b) Re_b = 1131, L/D = 53.2

(c) Re_b = 1697, L/D = 1.2 (d) Re_b = 1697, L/D = 53.2

(e) Re_b = 2263, L/D = 1.2 (f) Re_b = 2263, L/D = 53.2

(g) Re_b = 2829, L/D = 1.2 (h) Re_b = 2829, L/D = 53.2

(i) Re_b = 3961, L/D = 1.2 (j) Re_b = 3961, L/D = 53.2

(k) Re_b = 11317, L/D = 1.2 (l) Re_b = 11317, L/D = 53.2

Fig. 2 Instantaneous images of jet flow in the near field downstream the pipe nozzle, *i.e.* $0 \leq x/D \leq 5$, for the two assessed length to tube diameter ratios $L/D = 1.2$ (*left*) and $L/D = 53.2$ (*right*) for Reynolds numbers $Re_b = \{1131, 1697, 2263, 2829, 3961, 11317\}$. Flow is from *left* to *right*

in the rotation in the main axis which is likely to affect the velocity along the centerline. In addition, the collapse of the surrounding mixing layer is also more evident compared with $Re_b = 1131$. At $Re_b = 2263$, similar phenomena take place involving larger vortices so that a stronger fluctuation of the centerline velocity is expected.

At $Re_b = 3961$, large scale vortex formation and pairing are still observable. Nevertheless, the structure coherence is less evident than for lower Reynolds numbers. Increasing the Reynolds number beyond $Re_b = 4000$ has for effect to limit the vortex size, and to quickly destroy them. Consequently, for the highest Reynolds numbers, the presence of large structures is not observed, and is replaced by small surrounding structures and turbulent flow behaviour.

In the next section, velocity measurements by single hot film anemometry are presented and discussed.

3.2 Characterisation of radial initial and axial centerline velocity profiles

Initial radial jet velocity profiles at the nozzles exit and axial velocity profiles along the jet centerline are quantified with respect to mean and turbulence velocity statistics. In addition, boundary layer characteristics of initial radial jet profiles are presented.

3.2.1 Initial mean radial velocity profiles

The distribution of the mean axial velocity across the tube exit is measured at $x/D \leq 0.04$. The hot film is displaced in the axial direction as outlined in Section 2.1 so that

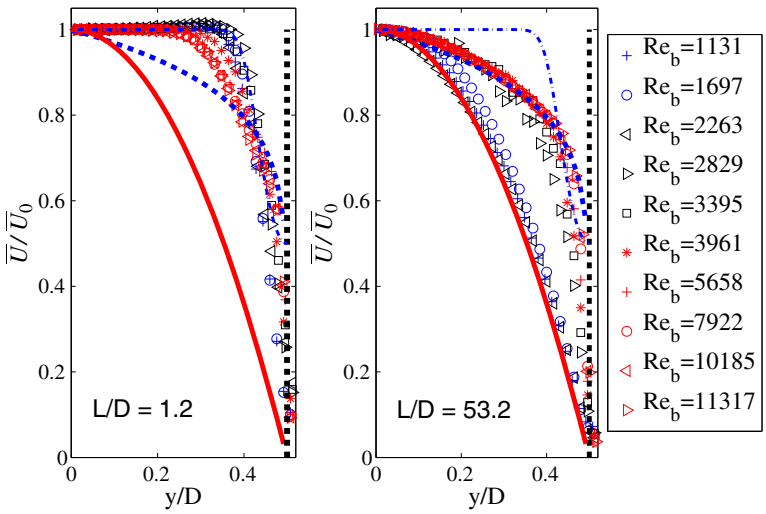

Fig. 3 Distribution of the mean axial velocity across the tube exit for $L/D = 1.2$ and $L/D = 53.2$ at $x/D \leq 0.04$ from the centerline $y/D = 0$ to the wall $|y/D| = 0.5$ (*vertical dashed line*). The velocity is normalised by the initial centerline velocity $\overline{U}_0$, *i.e.* $\overline{U}/\overline{U}_0(y/D)$. Profiles for Reynolds numbers $Re_b \in \{1131, 1697, 2263, 2829, 3961, 4527, 5658, 7922, 10185, 11317\}$ are shown. Measured profiles are compared to three empirical velocity profiles summarised in Table 2: parabolic profile (*full line*), 1/7 power law profile (*dashed line*) and 'top hat' profile with $\delta^{**} = 0.02D$ (*dash dot line*)

the measured jet radial profiles, $-0.7 < y/D < 0.7$, cover the tube exit diameter. The measured radial jet profiles are symmetric so that in the following only half jet profiles are shown. Normalised initial mean radial velocity profiles at the nozzle exit are illustrated in Fig. 3 for a limited number of Reynolds numbers. Measured profiles are compared to 3 empirical velocity profiles summarised in Table 2 [39]: parabolic profile, 1/7 power law profile and a hyperbolic tangent 'top hat' profile with momentum thickness $\delta^{**} = 0.02D$, with δ^{**} defined as:

$$\delta^{**} = \int_0^{D/2} \frac{\overline{U}(y)}{\overline{U}_0} \left(1 - \frac{\overline{U}(y)}{\overline{U}_0}\right) dy, \tag{3}$$

where $\overline{U}_0$ denotes the mean initial centerline velocity at the exit.

Normalised mean velocity profiles for $L/D = 53.2$ approximate a parabolic profile for Reynolds numbers $Re_b \leq 2263$ corresponding to fully developed laminar pipe flow [39, 44]. As the Reynolds number increases flow instabilities grow resulting in a turbulent pipe flow. Consequently, for $Re_b \geq 2829$ the mean velocity profile can be approximated by a turbulent 1/7th power law profile in the range, $0 \leq y/D \leq 0.4$ confirming observations for pipe flow [27, 45]. The observed transition from laminar to turbulent in the range $2000 < Re_b < 3000$ is in accordance with the flow visualisation shown in Section 3.1. It is seen that a core region with uniform velocity is absent for all Reynolds numbers so that the boundary layer dominates the flow.

Normalised initial radial mean velocity profiles for $L/D = 1.2$ do exhibit a core region with uniform velocity for all Reynolds numbers so that the initial boundary layer is confined to the near wall region. Consequently, compared to $L/D = 53.2$ the extent of the boundary layer is reduced and the exit profile is flattened in the core region as in case of a smooth contraction nozzle [27, 40, 45]. In addition, the influence of Reynolds number on the shape of the initial mean velocity profile is less pronounced for $L/D = 1.2$ than for $L/D = 53.2$. Indeed, the initial mean velocity profile for $L/D = 1.2$ can be approximated by a 'top hat' profile for all Reynolds numbers in case a non vanishing momentum thickness $\delta^{**} \neq 0$ is accounted for. From the shown radial mean velocity profiles, the momentum thickness is expected to increase with Reynolds number since the uniform core extent decreases from $0 \leq y/D \leq 0.35$ to $0 \leq y/D \leq 0.25$. Although the size of the uniform core extent is similar for a smooth contraction nozzle the momentum thickness is expected to decrease with Reynolds number [14]. Consequently, the presence of vortices immediately downstream the nozzle exit (shown in Section 3.1) and/or the upstream presence of sharp contraction edges affects the observed initial radial mean velocity profile compared to a smooth contraction nozzle since the dynamics of the boundary layer characteristics are altered.

Table 2 Empirical mean radial velocity profiles with $\overline{U}(y)$ the mean velocity at the radial position y, $\overline{U}_0$ the initial centerline velocity at $(x/D = 0, y/D = 0)$, tube diameter D and momentum thickness δ^{**}

Velocity profiles		
Parabolic	1/7 Power law	'Top hat'
$\overline{U}(y) = \overline{U}_0 \left[1 - \left(\frac{2\lvert y\rvert}{D}\right)^2\right]$	$\overline{U}(y) = \overline{U}_0 \left(1 - \frac{2\lvert y\rvert}{D}\right)^{1/7}$	$\overline{U}(y) = \frac{\overline{U}_0}{2} \left[1 - \tanh\left[\frac{1}{4}\frac{D}{2\delta^{**}}\left(\frac{2\lvert y\rvert}{D} - \frac{D}{2\lvert y\rvert}\right)^2\right]\right]$

3.2.2 Initial radial turbulence intensity profiles

The distribution of the radial turbulence intensity across the tube exit $T_U(y/D)$ is shown in Fig. 4. For $Re_b = 1131$, a constant radial turbulence intensity $T_U < 1$ % is observed from $y/D = 0$ up to the wall vicinity for both $L/D = 1.2$ and $L/D = 53.2$. As the Reynolds number increases significant differences appear between the initial turbulence profiles for $L/D = 1.2$ and $L/D = 53.2$.

For $L/D = 53.2$ and $1131 \leq Re_b \leq 1697$ a constant radial turbulence intensity $T_U < 1$ % is observed from $y/D = 0$ up to the wall vicinity. For $2263 \leq Re_b \leq 2829$, the initial turbulence intensity T_U increases which is likely associated with the generation and instability of large coherent structures downstream or/and upstream the tube exit. The range of Reynolds numbers for which the transition occurs corresponds well to a critical value of $Re_b \approx 2000$ for the onset of transition reported in [44] as well as with the onset of turbulence in the range $2000 < Re_b < 2700$ reported in [43] in presence of an orifice plate at the pipe inlet resulting in a large perturbation of the flow. As the Reynolds number increases further $3395 \leq Re_b \leq 11317$ the turbulence intensity at the pipe exit decreases. The observed initial profiles are in accordance with profiles observed for pipe flows [27]. The jump in initial turbulence intensity at $2263 \leq Re_b \leq 2829$ is in accordance with the transition from a laminar parabolic profile to a turbulent power law profile observed on the initial radial mean velocity profile.

For $L/D = 1.2$, a constant radial turbulence intensity $T_U < 1$ % from $y/D = 0$ up to the wall vicinity is only observed for the lowest Reynolds number $Re_b = 1131$. For $Re_b = 1697$ the turbulence intensity slightly increases to $T_U \approx 2$ %. Near the wall the turbulence intensity is reduced with about 1.5 %. For $2263 \leq Re_b \leq 3961$ flow

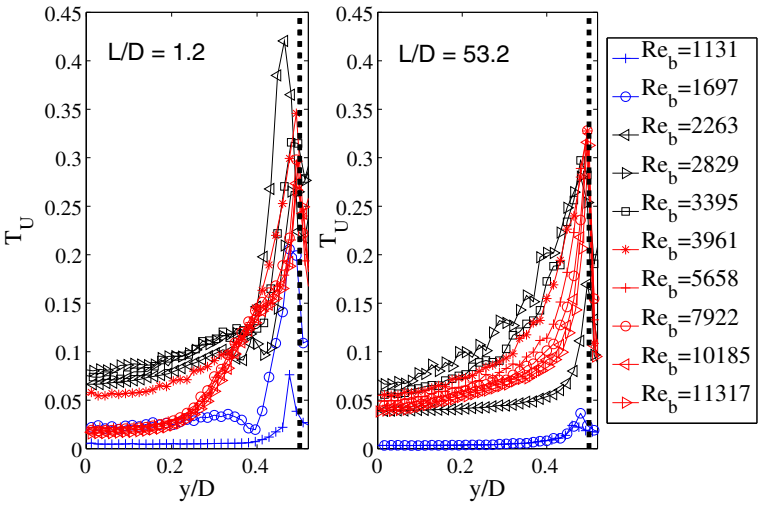

Fig. 4 Distribution of the axial turbulence intensity across the tube exit $T_U(y/D)$ for $L/D = 1.2$ and $L/D = 53.2$ at $x/D \leq 0.04$ from the centerline $y/D = 0$ to the wall $|y/D| = 0.5$ (*vertical dashed line*). Profiles for Reynolds numbers $Re_b \in \{1131, 1697, 2263, 2829, 3961, 4527, 5658, 7922, 10185, 11317\}$ are shown

instability increases, as illustrated by the pairing and deformation of coherent structures shown in Fig. 2, resulting in a sudden increase of the turbulence intensity which reaches a maximum for $Re_b = 2829$. As the Reynolds number increases further to within $5658 \leq Re_b \leq 11317$, the turbulence intensity drops and approximates $T_U \approx 2$ % in the core region with constant mean velocity for $0 \leq y/D \leq 0.25$. Outside the core region the turbulence intensity grows rapidly. The initial turbulence intensity profiles approximate the profile illustrated in [23, 40] for a smooth contraction nozzle although the core region is reduced due to the presence of sharp edges at the contraction inlet confirming observations made for a sharp edged orifice nozzle [34].

The initial centerline turbulence intensity, $T_{U,0}(y/D = 0, x/D = 0)(Re_b, L/D)$, is further analysed in Fig. 5 as function of Reynolds number Re_b. A sharp peak in initial turbulence intensity is observed in the range $2300 < Re_b < 3000$ for $L/D = 53.2$ and a broad peak in the range $2000 < Re_b < 4000$ for $L/D = 1.2$. The maximum of the peak occurs at approximately $Re_b \approx 2829$ for both $L/D = 1.2$ and $L/D = 53.2$. The peak in turbulence intensity covers the range of Reynolds numbers associated with flow instability and the deformation of coherent structures as illustrated in Fig. 2. Consequently, the broadening of the peak for $L/D = 1.2$ compared to $L/D = 53.2$ reflects the increased range of Reynolds numbers associated with the transition from stable flow to turbulent flow for $L/D = 1.2$ compared to $L/D = 53.2$. The increase of initial turbulence intensity associated with the transition regime is previously observed in case of coherent structure interaction for round jets [15]. Although from the current data it can not be concluded that the increase is due the same feedback mechanism as for round jets or/and that the increase is due the dynamics of upstream coherent structures associated with the upstream sharp edged contraction.

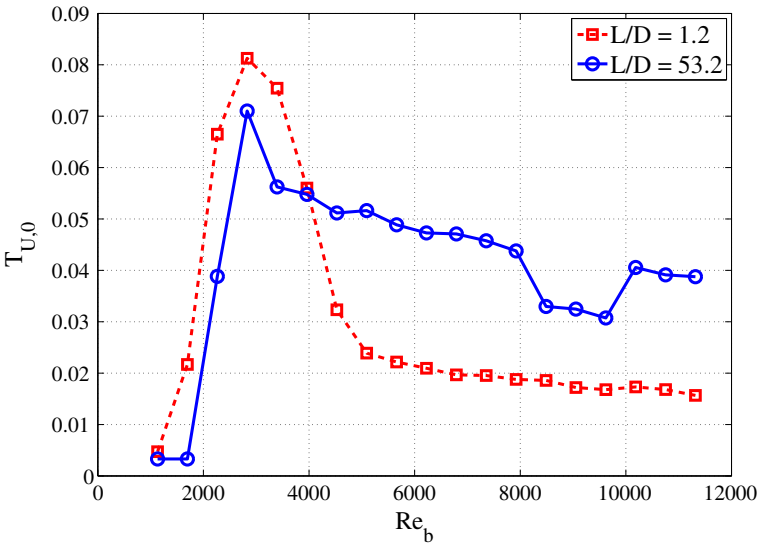

Fig. 5 Centerline turbulence intensity at the tube exit as function of Reynolds number Re_b, $T_{U,0}(y/D = 0, x/D \leq 0.04)(Re_b)$, for $L/D = 1.2$ and $L/D = 53.2$

For higher Reynolds numbers for which a breakdown of coherent structures in small scale structures is observed from Fig. 2, the turbulence intensity $T_{U,0}$ decreases and converges towards an asymptotic value of ≈3 % in case of $L/D = 1.2$ and of ≈1.6 % in case of $L/D = 53.2$.

The observed initial centerline turbulence intensities $T_{U,0}$ approximate values reported in [23] who studied the flow from a smooth contraction nozzle with equal length to diameter ratio and large contraction ratio. Since $T_{U,0}$ values are only given for a single Reynolds number $Re_b = 5500$ in [23], the evolution of $T_{U,0}$ as function of Reynolds number can not be discussed based on their data. No peak in initial turbulence levels $T_{U,0}$ is reported in [40] for a smooth contraction nozzle and $850 \leq Re_b \leq 5400$. In [40], the flow is maintained laminar at the exit of the contraction nozzle for all assessed Reynolds numbers due to the absence of coherent structures at the nozzle exit so that $T_{U,0} < 1$ % holds as for $Re_b = 1131$ in the current study.

Consequently, the presence of sharp edges at the contraction inlet triggers the instability of large coherent structures in the transition regime for $L/D = 1.2$ as well as for $L/D = 53.2$ resulting in a peak in the initial centerline turbulence level as function of Reynolds number whose width is determined by the extent of the transition region and whose amplitude is likely to depend on the feedback of coherent structure formation among others determined by the location of initial roll up of the vorticity layer.

3.2.3 Initial boundary layer characterisation

Initial radial mean velocity profiles at the tube exit, $x/D \leq 0.04$, are further analysed by considering the evolution of boundary layer parameters illustrated in Fig. 6: boundary layer thickness δ_{95}, momentum thickness δ^{**} defined in Eq. 3 and displacement thickness δ^{*}:

$$\delta^{*} = \int_0^{D/2} \left(1 - \frac{\overline{U}(y)}{\overline{U}_0}\right) dy, \tag{4}$$

where $\overline{U}_0$ indicates again the initial mean centerline velocity at the nozzle exit.

In accordance with the distribution of the mean radial velocity at the tube exit shown in Fig. 3, $L/D = 1.2$ is characterised by a thin boundary layer of approximately 10 % of the diameter D for $Re_b < 3000$, corresponding to the range for which the initial centerline turbulence intensity $T_{U,0}$ raises to its peak value as shown in Fig. 5. The thin boundary layer is associated with normalised momentum thickness $50 \leq D/\delta^{**} \leq 65$ and shape factor $1.8 < H_f < 2$. Increasing the Reynolds number in the range $3000 < Re_b < 6000$, for which the initial turbulence intensity $T_{U,0}$ decreases from 9 to ±2 %, induces a thickening of the boundary layer to approximately 20 % of the diameter D, a decrease of $D/\delta^{**} > 50$ to $D/\delta^{**} \approx 40$ and a reduction of $H_f > 1.8$ to $H_f \approx 1.5$, which approaches H_f values associated with turbulent flow. For $Re_b > 6000$, the flow remains nearly turbulent so that the flow regime is established and δ_{95}/D, D/δ^{**} and H_f become independent of Reynolds number Re_b.

For $L/D = 53.2$ and $Re_b < 2500$ the flow is characterised by a thick boundary layer for which $\delta_{95} \approx 0.35D$, $D/\delta^{**} \approx 19$ and $H_f \approx 1.95$. For $2500 < Re_b < 3000$ the boundary layer thickness decreases slightly with 5 %. In addition, the ratio D/δ^{**}

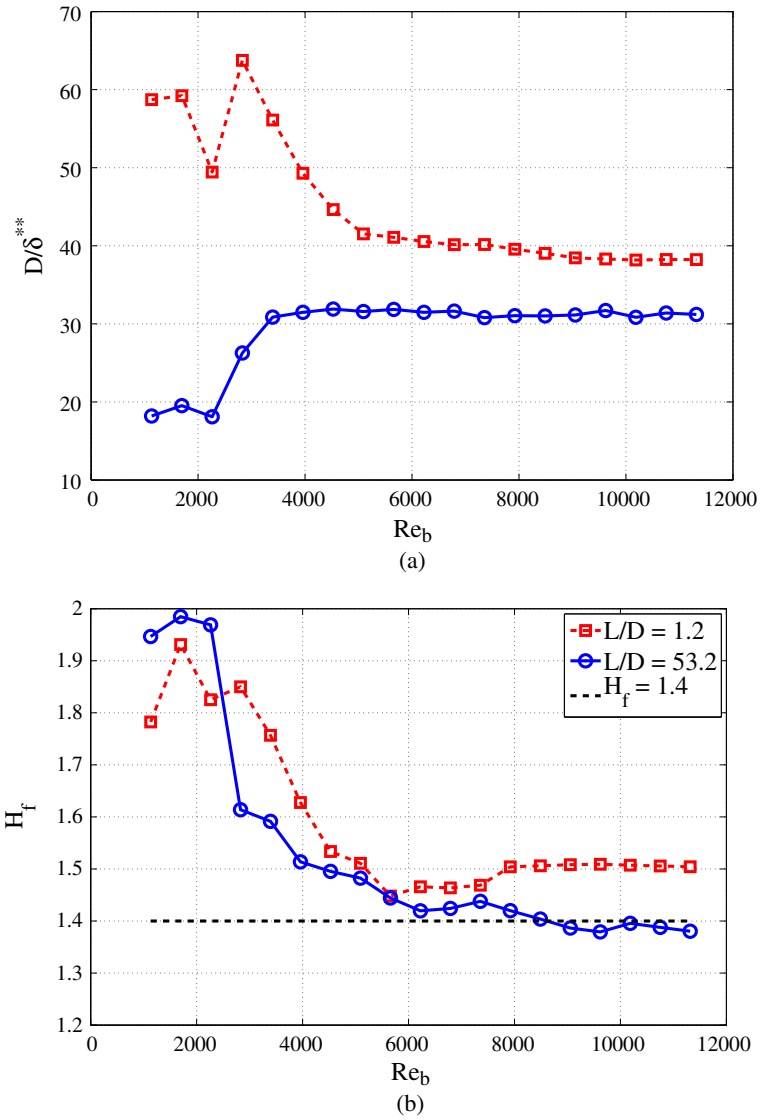

Fig. 6 **a** inversed momentum thickness D/δ^{**} and **b** shape factor H_f for $L/D = 1.2$ and $L/D = 53.2$ as function of Reynolds number Re_b. The *dashed vertical line* in Fig. 6b indicates $H_f = 1.4$ associated with turbulent pipe flow

increases rapidly to $D/\delta^{**} \approx 28$ and the shape factor drops to $H_f \approx 1.6$. The rapid variation of boundary layer characteristics coincides with the transition regime for which a peak in initial turbulence intensity $T_{U,0}$ is observed from Fig. 5. Increasing the Reynolds number further to $Re_b > 3000$ does not induce any rapid changes. The boundary layer thickness increases gradually with 1 % to $\delta_{95} \approx 0.31D$. The value of D/δ^{**} reaches its asymptotic value at $D/\delta^{**} \approx 31$ and the shape factor reduces until

it reaches its asymptotic value at $H_f \approx 1.4$ in accordance with fully turbulent pipe flow [43, 44].

Consequently, the abrupt contraction at the tube inlet prevents, both for $L/D = 1.2$ and for $L/D = 53.2$, a laminar boundary layer to occur based on the shape factor which never reaches $H_f = 2.5$ associated with Blasius theoretical laminar boundary layer velocity profile. The resulting boundary layers are concluded to be transitional until $Re_b > 6000$ for $L/D = 53.2$ and for all assessed Reynolds numbers $Re_b \leq 11317$ for $L/D = 1.2$. Consequently, in case of $L/D = 1.2$, a fully turbulent initial boundary layer is prevented due to upstream presence of the abrupt contraction at the tube inlet resulting in the possible generation of large coherent structures upstream the tube exit which do not break down completely or/and due to the feedback of coherent structures generated downstream the tube exit.

Moreover D/δ^{**} values for $L/D = 1.2$ are larger than values observed for $L/D = 53.2$ and consequently the momentum thickness for $L/D = 53.2$ is larger than the momentum thickness for $L/D = 1.2$ in accordance with the initial mean radial velocity profiles shown in Fig. 3. Experimental studies and linear stability analysis of the round jet behavior in the near field suggest that for high values of $D/\delta^{**} \approx 100$ an azimuthal axisymmetrical instability of the shear layer results in ring vortices immediately downstream the jet axis $0.04 \leq x/D \leq 1$ and that as the ratio D/δ^{**} decreases more downstream, $x/D \geq 1$, the azimuthal sinuous instability is most prominent resulting in helical vortices [6, 8, 29]. From the flow visualisation, shown in Fig. 2, it is seen that for $L/D = 53.2$, for which $D/\delta^{**} < 35$ holds, such helical vortices are indeed observed supporting the findings in [6, 8, 29]. For $L/D = 1.2$ on the other hand no helical vortices can be observed regardless the value of D/δ^{**}, $35 < D/\delta^{**} < 70$. Consequently, it is seen that the presence of sharp upstream edges at the entrance of the abrupt constriction triggers the axisymmetrical shear layer instability at the tube exit and therefore the formation of toroidal ring vortices for all assessed D/δ^{**}.

3.2.4 Centerline mean velocity

Figure 7 presents the centerline variation of the mean velocity $\overline{U}_c(x, y/D = 0)$ normalised by the initial centerline velocity $\overline{U}_0(x = 0, y/D = 0)$ in the near field region $0 < x/D < 5$ for $L/D = 1.2$ and $L/D = 53.2$.

For $L/D = 53.2$, the near field centerline mean velocity decreases for all assessed Reynolds numbers, which is in contrast with observations reported in [2, 3, 7, 19, 27] on a smooth long pipe nozzle. Since probe alignment is verified before and after each flow measurement the initial mean velocity decay is not due to a measurement error. Instead a slight decrease in velocity is observed in case of forced jets [7] for $Re_b \approx 10^5$. Therefore, it is suggested that the presence of sharp edges at the pipe inlet due to the abrupt contraction induces jet forcing. Although the forcing is observed for all Reynolds numbers, the decay increases for Reynolds numbers associated with the transition region $2263 \leq Re_b \leq 2829$, e.g. 2 % at $x/D = 3$ for $Re_b = 1131$ up to 4 % at $x/D = 3$ for $Re_b = 2829$.

For $L/D = 1.2$, the mean centerline velocity reduces downstream from the pipe exit, suggesting a forced jet as observed for $L/D = 53.2$. For Reynolds numbers outside the transition range, *i.e.* for $Re_b = 1131$ and $Re_b > 3961$ the magnitude of the decay does not exceed the order of magnitude for $L/D = 53.2$, e.g. the decay yields 2 % at $x/D = 3$ for $Re_b = 1131$. Moreover, a severe 25 % centerline

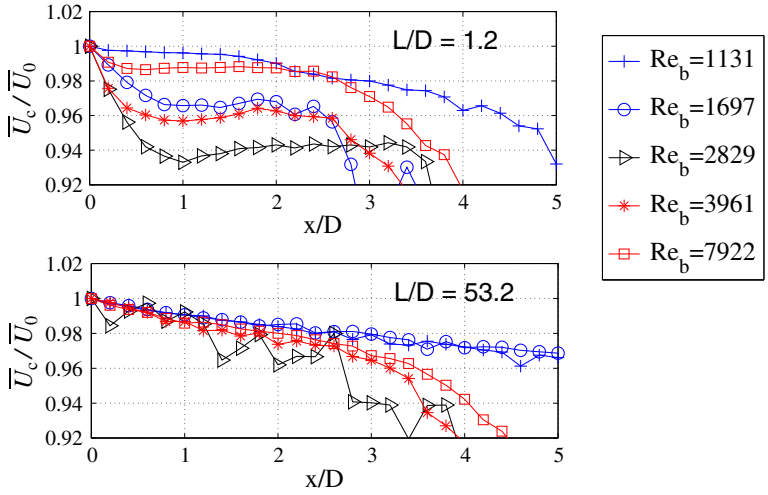

Fig. 7 Illustration of normalised centerline mean velocity $\overline{U}_c/\overline{U}_0$ in the near field $0 < x/D < 5$ for $L/D = 1.2$ and $L/D = 53.2$

velocity increase immediately downstream the exit, which characterises an orifice round jet [3, 7, 19, 34, 40] due to the *vena contracta* effect, is not observed in the current study confirming that such an effect is damped out within 0.5 diameters downstream from the abrupt contraction at the nozzle inlet. For Reynolds numbers in the transition range $1697 \leq Re_b \leq 3961$ the centerline velocity shows a much more complex behaviour than observed for $L/D = 53.2$. Indeed, the decay varies as function of Reynolds number and as function of downstream distance x/D since an initial velocity reduction in $0 \leq x/D \leq 1$ is followed by a downstream zone of almost constant velocity for $1 < x/D < 3$. In the transitional flow regime $1131 < Re_b \leq 3961$, associated with a broad peak in initial centerline turbulence intensity $T_{U,0}$ shown in Fig. 5, the initial velocity reduction at $x/D = 1$ varies between 3 and 7 %. The largest initial velocity reduction of 7 % is obtained for $Re_b = 2829$ at $x/D = 1$, which is associated with the highest initial centerline turbulence intensity $T_{U,0}$ as well as with the highest diameter to momentum thickness ratio D/δ^{**} as shown in Fig. 6a. Moreover, the flow visualisation study shown in Fig. 2 illustrates that for $Re_b = 2829$ $x/D \approx 1$ corresponds to the region of tailing vortex formation which is followed by vortex pairing further downstream. Therefore, the visualisation study as well as the quantified initial conditions suggest that the initial velocity reduction is due to the formation and interaction of large coherent structures, which suggests self excitation of the jet [15]. A velocity reduction due to vortex development is also observed for a smooth contraction nozzle for Reynolds number in the range $1620 < Re_b < 4050$ [40]. Nevertheless, the presence of upstream sharp edges due to the abrupt contraction approaches the downstream extent of velocity reduction closer to the jet exit $0 < x/D \leq 1$ compared to $0 < x/D < 4$ reported in [40] for a smooth contraction nozzle.

The potential core extension x_{pc}, defined as the downstream position where the centerline velocity $\overline{U}_c = 0.95\overline{U}_0$, is plotted in Fig. 8. For both $L/D = 1.2$ and

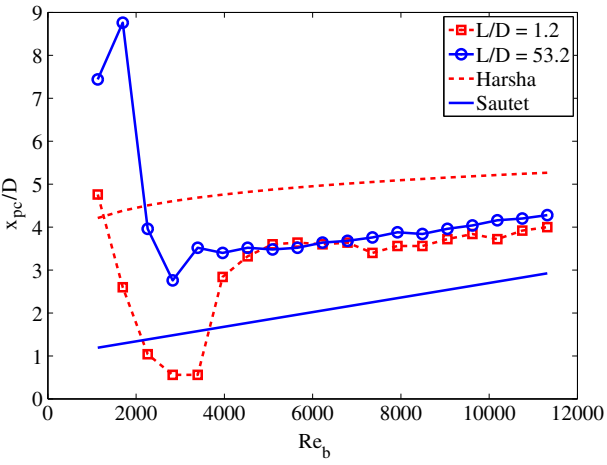

Fig. 8 Normalised potential core extent x_{pc}/D for $L/D = 1.2$ and $L/D = 53.2$ as function of Reynolds number Re_b. As a reference *ad hoc* relationships [16, 38] for a smooth contraction nozzle and high Reynolds number are shown as well

$L/D = 53.2$ the potential core extent decreases as the Reynolds number increases from $Re_b = 1131$, as observed in [21], as long as the associated initial turbulence intensity $T_{U,0}$, shown in Fig. 5, increases as well. Consequently, a minimum potential core length is obtained for $Re_b = 2829$ for which the initial turbulence intensity $T_{U,0}$ is maximum for both $L/D = 1.2$ and $L/D = 53.2$. For $Re_b > 2829$ the potential core extent increases during the transitional flow regime until the initial turbulence intensities observed for $L/D = 1.2$ and $L/D = 53.2$ are in close agreement. For $Re_b > 4000$, the potential core slowly increases with Reynolds number for both $L/D = 1.2$ and $L/D = 53.2$ as observed in [2, 24, 33]. Consequently, for Reynolds numbers $Re_b < 4000$ the potential core length shortens under influence of viscous forces driving vortex formation and interaction whereas for $Re_b > 4000$ inertial forces determine the potential core extent. The qualitative behaviour of x_{pc} for $Re_b > 4000$ corresponds to the *ad hoc* relationships $x_{pc}(Re_b)$ for smooth contraction nozzles described by Harsha [16] for $Re_b > 1.2 \times 10^4$ and by Sautet and Stepowsky [38] for $4700 \leq Re_b \leq 2.7 \times 10^4$. Moreover, the flow visualisation shown in Fig. 2 illustrates the shortening of the potential core extent x_{pc} at the onset of flow instabilities and the formation of large coherent structures. For $L/D = 53.2$, x_{pc} reduces with a factor 2 between $Re_b = 1697$ and $Re_b = 2263$ although the initial turbulence intensity is of the same order of magnitude as shown in Fig. 5. For $L/D = 1.2$, enhanced instability of the coherent structures reduces the potential core extent x_{pc}, as seen e.g. when comparing $Re_b = 1697$ and $Re_b = 2263$ in Fig. 2, although following Fig. 5 in this case the initial turbulence intensity $T_{U,0}$ increases as well.

Although not explicitely discussed in [40], from the presented data in Fig. 8 is observed that the potential core extent $x_{pc}(Re_b)$ for a smooth contraction nozzle follows tendencies observed in the current study for an abrupt contraction and $L/D = 1.2$. The initial potential core extent x_{pc} decreases as the Reynolds number Re_b is increased from $Re_b \approx 10^3$ due to the occurrence of large coherent structures until $Re_b \approx 2 \times 10^3$. As the Reynolds number increases further, the potential core extent increases as well. Nevertheless, values $x_{pc}/D \approx 3$ found for an abrupt contraction in the range $Re_b > 4000$ are smaller than $x_{pc}/D \geq 5$ derived from data presented

in [40] for a smooth contraction nozzle. Consequently, the potential core extent is shortened compared to a smooth contraction nozzle.

3.2.5 Centerline turbulence intensity

For $L/D = 1.2$ one or more (in case of $Re_b = 2829$) humps with a well defined peak turbulence intensity between 12 % and 19 % appear for $x/D \leq 5$ and Reynolds numbers in the transitional regime $1131 < Re_b < 4527$ as illustrated in Fig. 9. The turbulence intensity humps are followed by a lowering. The humps in the near field are associated with the presence of large scale structures and consequently do not occur for $L/D = 53.2$ since no such structures are present in the near field. It is seen that as the Reynolds number increases to $Re_b = 2829$, and so does the maximum initial mean turbulence intensity $T_{U,0}$ as observed from Fig. 5, the peak intensity of the humps increases and its spatial position shifts downstream from $x/D \approx 0.7$ to $x/D \approx 1$ for which large coherent structures are indeed observed in Fig. 2. An increase of Reynolds number, $Re_b > 4527$, leads to a disappearance of the hump since no large structures occur.

The presence of a hump in the axial turbulence intensity was previously observed for a smooth contraction nozzle [7, 27, 40]. The downstream position and the intensity of the turbulence peak varies considerably: $4 \leq x/D \leq 4.75$ [40], $x/D \approx 6$ [27] and $2 < x/D < 7$ [7]. The peak amplification depends on Reynolds number and on coherent structures present in the jet. In the current study, the upstream presence of sharp edges at the inlet provokes a generation of toroidal ring vortices immediately downstream from the tube exit with a short spatial lifespan compared to [7, 27, 40]. Therefore, the peak turbulence position occurs closer to the tube exit. An

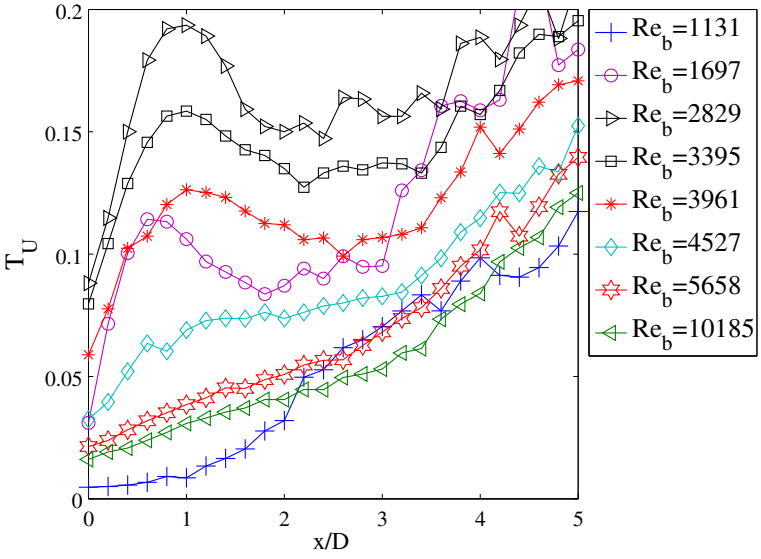

Fig. 9 Centerline turbulence intensity $T_U(x/D)$ in the near field for $L/D = 1.2$

amplification of the maximum peak value with Reynolds number as found by [40] is not observed in the current study since the boundary layer thickness is not constant for all Reynolds numbers, $\delta_{95} \approx 0.1D$ holds for $850 \leq Re_b \leq 6750$ in [40]. Instead, the boundary layer thickens with Reynolds number from $\delta_{95} \approx 0.1D$ at $Re_b = 2258$ to $\delta_{95} \approx 0.2D$ for $Re_b > 5658$, which stabilises the boundary layer. In addition, the current study is characterised by a transition from laminar to turbulent flow which is not the case in [40], so that in [40] large coherent structures are observed at all Reynolds numbers, whereas a breakdown of coherent structures is observed in the current study for $Re_b > 4000$.

3.3 Temporal and spectral analysis of the velocity signal

Flow visualisation and characterisation of the measured velocity profiles show that the formation and dynamics of coherent structures in the near field downstream from the nozzle exit determine the jet flow development to a large extent. Therefore, in the current section, temporal and spectral features of the velocity in the initial shear layer at the nozzle exit and along the centerline velocity in the range $0 < x/D \leq 5$ are presented for $L/D = 1.2$ and $L/D = 53.2$.

3.3.1 Temporal analysis

For $L/D = 1.2$ and $Re_b = 1131$, the instantaneous centerline velocity is characterised by the apparition of a quasi periodical fluctuation as the flow moves downstream from $x/D \leq 0.04$ to $x/D = 1$, the fluctuation reduces further downstream as seen at $x/D = 5$. As the Reynolds number increases to $Re_b = 1697, 2263$ a strong regular quasi periodical fluctuation is obtained at $x/D \leq 0.04$. The same way as for $Re_b = 1131$ the fluctuation is amplified at $x/D = 1$ and looses its quasi periodicity at $x/D = 5$. Further increasing of the Reynolds number results in an absence of a quasi periodical fluctuation at all measurement stations as illustrated for $Re_b = 11317$. The evolution of the fluctuating velocity signal $U_p(t)/\bar{U}_0$, with physical time t, for $L/D = 1.2$ is illustrated for $Re_b = 2263$ in Fig. 10.

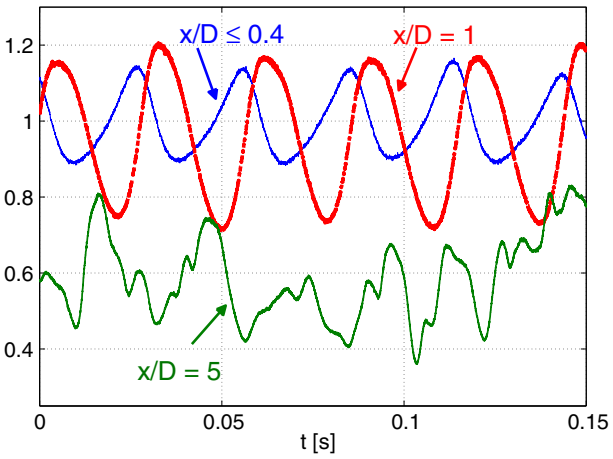

Fig. 10 Illustration of a 0.15 s sequence of normalised instantaneous velocity $U_p(t)/\bar{U}_0$ for $L/D = 1.2$ at downstream centerline positions $x/D \leq 0.04$, $x/D = 1$ and $x/D = 5$ for Reynolds number $Re_b = 2263$

In general, a quasi periodic fluctuation of the temporal velocity signal occurs in the downstream region for $L/D = 1.2$ for Reynolds numbers for which large coherent structures are observed in Fig. 2. Consequently, no quasi periodic fluctuations are observed for $Re_b = 11317$. Moreover, the fluctuation amplifies for Reynolds numbers in the transitional regime, $1132 < Re_b \leq 4527$ corresponding to the peak in initial turbulence shown in Fig. 5. The measurement station situated just downstream the potential core extent at $x/D = 5$, since $x_{pc}/D \leq 4$ holds for $L/D = 1.2$ as shown in Fig. 8, bears only traces of the quasi periodicity since the shear layers collapses outside the potential core so that vortices break down rapidly and turbulence is created. Flow visualisation results as shown in Fig. 2 suggest that the amplification of the quasi periodic fluctuation between $x/D \leq 0.04$ and $x/D = 1$ as well as the amplification with Reynolds number is due to growing of unstable vortices nearest to the centerline so that the radial extent of the jets central core decreases and the centerline velocity becomes more affected by the passing and interaction of vortices. For $Re_b = 1131$ the Reynolds number is sufficiently low so that the jet shear layer structures are only marginaly unstable which limits their growth [1, 8]. Consequently, the hump in axial turbulence intensity before the potential core onset as observed in this study for $L/D = 1.2$ in Fig. 9 and reported for a contraction jet in among others [7, 27, 40] is indeed due to the passage of unstable large scale coherent structures and not to the creation of real small scale and random velocity fluctuations. The coherent structures observed for the lowest Reynolds number $Re_b = 1131$ are stable and hence no hump in centerline turbulence can be observed.

3.3.2 Spectral analysis

A spectral analysis of the instantaneous velocity is assessed for $L/D = 1.2$ and $L/D = 53.2$ in order to observe the flow dynamics in more detail. Non dimensional frequencies or Strouhal numbers are derived from the bulk velocity and the tube diameter D denoted $St_D = \frac{fD}{U_b}$ and from the bulk velocity and momentum thickness denoted $St_{\delta^{**}} = \frac{f\delta^{**}}{U_b}$.

From the flow visualisation, temporal analysis and velocity characterisation, it is seen that the presence and/or absence of stable and unstable large coherent structures in the jet shear layer determines the jet dynamics for both $L/D = 1.2$ and $L/D = 53.2$. Consequently, in order to increase understanding of jet dynamics the initial shear layer spectral properties of the velocity are analysed at $y/D = 0.5$ and $x/D \leq 0.04$. Resulting spectra for $L/D = 1.2$ and $L/D = 53.2$ are illustrated in Fig. 11.

For $L/D = 1.2$, sharp energy peaks appear for $1131 \leq Re_b \leq 2829$ corresponding to quasi periodical temporal shear layer fluctuations induced by the passage of ring vortices, which are seen to be present at the nozzle exit. The physical frequency f of the highest energy peak increases slightly with Reynolds number in the range $27 \leq f \leq 37$ Hz. The corresponding Strouhal numbers St_D therefore decrease with Reynolds number from 1.1 to 0.5. The spectra broaden as the Reynolds number increases in the range $1131 \leq Re_b \leq 2829$ due to the breakdown of vortices and increase of turbulence as the jet becomes more and more unstable. The increase in instability of the initial jet shear layer is also revealed by the appearance and growth of harmonics of the fundamental peak frequency. A first harmonic appears for $Re_b = 1697$ and two harmonics are observed for $Re_b = 2263$ and $Re_b = 2829$.

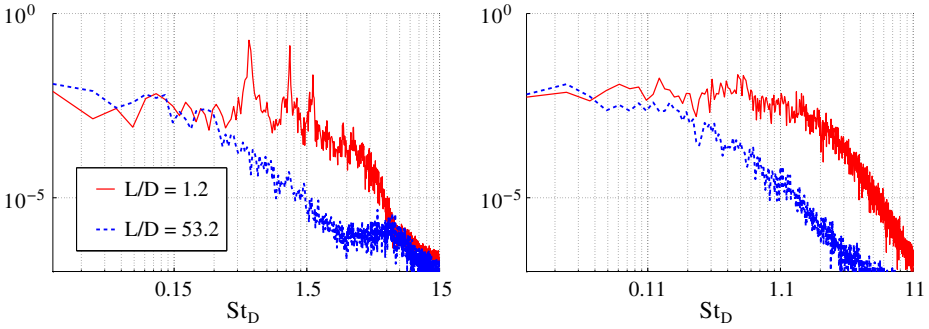

Fig. 11 Initial shear layer velocity power spectra, at measurement station ($x/D \leq 0.04$, $y/D = 0.5$), for Reynolds numbers $Re_b = 2829$ and $Re_b = 3961$ for $L/D = 1.2$ (*full line*) and $L/D = 53.2$ (*dashed line*). The spectra for $L/D = 53.2$ are shifted downwards with respect to spectra for $L/D = 1.2$

It is well established that the occurrence of harmonics characterises non linearities associated with the creation of turbulence highlighting the nonlinear near field region featuring unstable structures [10, 42]. In addition, the presence of smaller and broader low frequency peaks illustrates the complexity of the flow in the transition regime. For $Re_b \geq 3961$ broad spectra associated with turbulent flow are observed for which the inertial part is small due to the moderate Reynolds numbers under study and no peaks are detected.

The broadening of the spectra is also observed for $L/D = 53.2$ so that for $Re_b = 11317$ the spectra for $L/D = 1.2$ and $L/D = 53.2$ are similar. Compared to $L/D = 1.2$, spectral broadening as function of Reynolds number is slowed down, which illustrates the increased stability of the initial shear layer for $L/D = 53.2$. In contrary to $L/D = 1.2$, no sharp energy peaks can be observed since the line peak observed for $1131 \leq Re_b \leq 2263$ correspond to measurement errors due to the 50 Hz network frequency. The absence of sharp peaks is in agreement with the flow visualisation shown in Fig. 2 where no coherent structures are observed in the initial shear layer for $L/D = 53.2$. Nevertheless, the presence of a broad low frequency peak is suggested for $Re_b \leq 2829$. Associated Strouhal numbers St_D yield between 0.25 and 0.31.

The power spectral density of the velocity signal in the near field for measurement stations along the centerline at $x/D = 1$, $x/D = 2$, $x/D = 3$, $x/D = 4$ and $x/D = 5$ is illustrated for $L/D = 1.2$ in Fig. 12. As a result of the rich spectral contents of the initial shear layer, illustrated in Fig. 11, the centerline spectra obtained for $L/D = 1.2$ are characterised by broad and/or sharp frequency peaks for which the spectral position and amplitude vary as function of Reynolds number Re_b and measurement station x/D. For $Re_b = 1131$, the spectra exhibit a broad frequency peak at approximately 14 Hz, corresponding to Strouhal number $St_D \approx 0.55$ for all measurement stations $1 \leq x/D \leq 5$. The amplitude of the broad peak amplifies as x/D increases to $x/D = 3$ and reduces at $x/D = 5$. The broad peak is associated with the roll up of the initial vorticity sheet into a toroidal vortex ring. The maintenance of the peak, regardless x/D, confirms the quasi stability of coherent structures for $Re_b = 1131$ as observed from flow visualisation in Fig. 2 as from the temporal

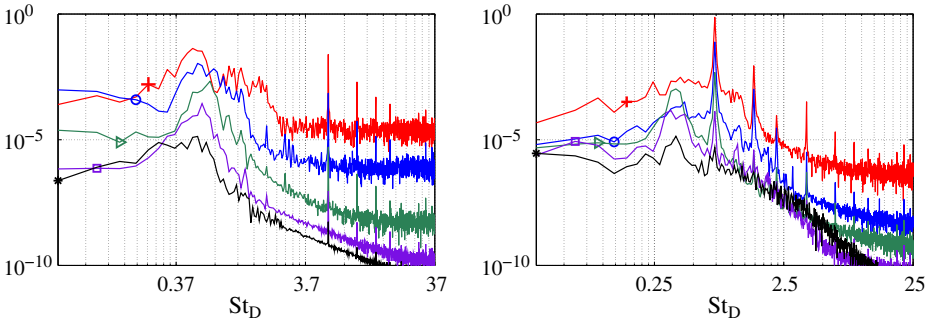

Fig. 12 Power spectra of centreline velocity signals for $L/D = 1.2$ and Reynolds numbers $Re_b = 1131$ and $Re_b = 1697$ at five downstream positions $x/D = 1$ (+), $x/D = 2$ (∘), $x/D = 3$ (▷), $x/D = 4$ (□), $x/D = 5$ (∗). Every spectrum is shifted downwards with respect to the previous

velocity signal. For $Re_b = 1697$, a sharp peak at 30 Hz appears comparable to those observed in the jet shear layer. In addition, harmonics are observed at $x/D = 1$ and $x/D = 2$. The presence of this sharp energy peaks in the centerline power spectrum confirms the formation of vortices and the convection of surrounding vortices at specific frequencies. A broad subharmonic emerges at approximately 15 Hz at $x/D \geq 3$ along with a reduced amplitude of the sharp energy peak and the disappearance of the harmonics. The appearance of the subharmonic is associated with the pairing of two ring vortices illustrated in Fig. 2. The general tendencies outlined for $Re_b = 1697$ are also observed for $2263 \leq Re_b \leq 3961$. The frequency of the peaks shifts to higher frequencies as the Reynolds number increases corresponding to an acceleration in the vortex generation resulting in increased instability and interaction of the coherent structures so that the amplitude of the peaks varies with Reynolds number. For $Re_b = 2263$ the amplitude of the peaks increases due to the reduced central jet portion so that the centerline velocity is most influenced by the passing of coherent structures and their interaction. For $2263 < Re_b \leq 3961$ the amplitude of the peaks, sharp as well as broad, gradually decreases so that for $Re_b = 2829$ the velocity spectrum is flattened out at $x/D = 5$. For $Re_b = 3961$ the spectra are flattened out at $x/D = 4$ and $x/D = 5$ resulting in spectra characteristic for turbulent flow. Finally, for $Re_b = 11317$ all spectra are flattened out, so that no well defined sharp peaks are observed.

In contrast to $L/D = 1.2$, power spectra along the centerline for $L/D = 53.2$ are not characterised by sharp energy peaks and so no fundamental and harmonics are observed. Instead for $Re_b = 1131$ a broad low frequency peak ($\approx 6Hz$) appears for $Re_b = 1131$ which approximates the Helmholtz frequency for $L/D = 53.2$ as indicated in Table 1. The amplitude of the peak increases as the Reynolds number increases from $Re_b = 1131$ to $Re_b = 2263$ in agreement with the visualisation of helical vortices for $Re_b = 2263$ shown in Fig. 2. A further increase of the Reynolds number flattens the power spectra for all measurement stations x/D for $Re_b \geq 3961$. For $L/D = 53.2$, the normalised boundary layer thickness δ_{95}/D yields values greater than those observed for $L/D = 1.2$. As a consequence, the jet shear layer is more difficult to disturb and the generation of large coherent structures is less pronounced and no toroidal ring vortices are generated.

Table 3 presents an overview of Strouhal numbers St_D characterising the centerline spectra for $L/D = 1.2$ and $L/D = 53.2$. The Strouhal number St_D is shown in order to compare with values reported for a smooth contraction nozzle given in [40]. Two peak values are reported on. The main frequency associated with vortex formation and the frequency after vortex pairing. The uncertainty on the reported values is due to low spectral resolution for low frequencies and to the variation of the peak frequency as the spatial measurement position is shifted downstream from $x/D = 1$ to $x/D = 5$.

For $L/D = 53.2$, St_D peaks are associated with main vortex formation since no vortex pairing is observed. The non dimensional frequencies St_D decreases as the Reynolds number increases from $St_D \approx 0.18$ to $St_D \approx 0.10$. The decrease in Strouhal number is due to the increase in bulk velocity since all frequency peaks approximate the Helmholtz frequency. Non dimensional frequencies associated with main vortex formation for $L/D = 1.2$ show the same Reynolds dependence since a decrease from $St_D \approx 0.7$ down to $St_D \approx 0.6$ is found. Consequently, Strouhal numbers St_D associated with $L/D = 1.2$ are a multiple of Strouhal numbers St_D for $L/D = 53.2$. The ratio $St_D(L/D = 1.2)/St_D(L/D = 53.2)$ increases from ≈ 3 for $Re_b = 1131$ to ≈ 6 for $Re_b = 2263$. The multiplication factor for low Reynolds numbers is partly explained by the difference in initial momentum thickness δ^{**}. Indeed, Fig. 6a shows that for $Re_b < 3000$ the momentum thickness for $L/D = 53.2$ yields approximately three times values observed for $L/D = 1.2$. Therefore, for $Re_b = 1131$ the Strouhal number based on the momentum thickness yields $St_{\delta^{**}} \approx 0.01$ for both L/D ratios. As the Reynolds number increases the Strouhal number based on the momentum thickness for $L/D = 1.2$ remains $St_{\delta^{**}} \approx 0.01$, which is in accordance with the order of magnitude of $St_{\delta^{**}}$ reported in [15] for transitional round jet flow at $Re_b = 15 \times 10^4$, whereas for $L/D = 53.2$ its value decreases due to the increase in bulk velocity. Consequently, the Reynolds dependence of vortex formation for $L/D = 53.2$ is more pronounced than for $L/D = 1.2$

For $L/D = 1.2$, Strouhal numbers St_D associated with vortex formation $0.6 < St_D < 0.71$, reported in Table 3, are higher than values $0.5 < St_D < 0.6$ reported in [40] for a smooth contraction nozzle. Since the boundary layer thickness at the tube exit yields $\delta_{95} \approx 0.1D$ in the current study as well as in [40] the found increase for the current study is due to the presence of sharp edges at the contraction inlet. In addition, found St_D values in the current study reduces with Reynolds number whereas values reported in [17, 40] show the opposite tendency. This finding suggests

Table 3 Overview of non dimensional frequencies or Strouhal numbers $St_D(Re_b, L/D)$ for centerline spectra for $L/D = 1.2$ and $L/D = 53.2$

Re_b	$L/D = 1.2$		$L/D = 53.2$	
	Pairing	Formation	Pairing	Formation
1131	–	0.6 ± 0.1	–	0.18 ± 0.05
1697	0.38 ± 0.05	0.71 ± 0.01	–	0.12 ± 0.03
2263	0.32 ± 0.01	0.63 ± 0.01	–	0.10 ± 0.01
2829	0.32 ± 0.01	0.61 ± 0.01	–	–
3961	–	0.60 ± 0.01	–	–

Shown values indicate the mean and standard variation obtained at different centerline measurement stations in the range $1 \leq x/D \leq 5$ for the non dimensional frequency after pairing and the non dimensional frequency associated with main vortex formation

that the influence of the upstream sharp edges on vortex formation decreases as the Reynolds number increases so that $St_D \approx 0.6$ for $Re_b \approx 4000$ in the current study as in well as in values reported in [40].

From Table 3, it is seen that in case of $L/D = 1.2$ non dimensional frequencies St_D associated with paired vortices yield half of values associated with vortex formation at the same Reynolds number, as expected for a subharmonic. The same observation is made in [40]. The retrieved values $St_D \approx 0.3$ correspond to the natural frequency observed for higher Reynolds number forced jets [7].

In general, spectra observed for $L/D = 1.2$ in the transitional regime $1131 < Re_b < 4000$ are shaped by vortex formation, appearance of harmonics, vortex pairing and finally vortex breakdown and entrainment. This description is in accordance with the two ring model for a transitional axisymmetrical jet at high Reynolds number $Re_b = 15 \times 10^4$ outlined in [15].

4 Conclusion

Jet dynamics in the near field downstream from an abrupt contraction with sharp edges coupled to a uniform circular tube extension with length to diameter ratio $L/D = 1.2$ and $L/D = 53.2$ is studied for moderate Reynolds numbers in the range $1131 < Re_b < 11320$. The presence of an abrupt contraction at the nozzle inlet disturbs the flow so that the jet becomes transitional for low Reynolds numbers in the range $1131 < Re_b < 4000$ for both assessed length to diameter ratios. As a consequence, the near field behaviour is dominated by the generation, passage and interaction of large flow structures associated with transition which results in a peak value of the initial centerline turbulence intensity $T_{U,0}$ around $Re_b \approx 2263$. For $Re_b > 2263$, the structures start to break down so that for higher Reynolds numbers $Re_b > 4000$ the jet dynamics becomes similar to observations made for high Reynolds numbers $Re_b > 10^4$ indicating that the jet dynamics becomes mainly determined by flow inertia and backflow [16, 38, 43].

In case of $L/D = 53.2$, helical vortices are suggested to occur for Reynolds numbers corresponding to the transition regime. Despite the decrease of transition Reynolds number, jet development for $L/D = 53.2$ in the laminar, transition and turbulent regime follows mainly tendencies described in these regimes for long pipe flow with $L/D \geq 40$. Nevertheless, it is observed that the mean centerline velocity in the near field decreases as is observed for forced jets.

For $L/D = 1.2$ the impact of the sharp contraction on the jet dynamics is more profound and the dynamics of main features such as the initial boundary layer development deflects from tendencies expected for smooth contraction nozzles. Indeed, it is shown that in contrast to a smooth contraction nozzle the momentum thickness of the trapezoidal velocity profile increases with Reynolds number until $D/\delta^{**} \approx 40$ due to the presence of large coherent structures immediately downstream from the nozzle exit, which is associated with a broad increase in initial turbulence centerline velocity associated with the transition regime $1131 < Re_b < 4000$ and decreased turbulence intensity in the near wall region in the range $1131 < Re_b < 3000$, whereas those phenomena are not observed in case of smooth contraction nozzles for which no transitional regime is observed. Smoke visualisation illustrates the formation of toroidal ring vortices in this range of Reynolds numbers. As the Reynolds number is

increased a secondary vortex appears in the tail of the first one and a vortex pairing phenomenon occurs. This observation is confirmed by the velocity power spectra for which a broad subharmonic and a sharp peak is found corresponding to vortex pairing and formation respectively. In addition, several harmonics of the main vortex formation frequency are observed which are associated with transition to turbulence and therefore not observed for smooth contraction nozzles [27, 40]. Moreover, compared to smooth contraction nozzles [27, 40] the spatial occurrence of formation of toroidal rings, their interaction and breakdown is shifted upstream towards the nozzle exit so that the flow dynamics for $L/D = 1.2$ in the transitional regime $1620 \leq Re_b \leq 4527$ can be described by the two ring model for axisymmetrical transitional high Reynolds number jets, $Re_b > 10^4$ [15], which explains the observed vortex pairing by self-excitation of the jet.

References

1. O'Neill, P., Soria, J., Honnery, D.: The stability of low Reynolds number round jets. Exp. Fluids **36**, 473–483 (2004)
2. Abdel-Rahman, A., Al-Fahed, S., Chakroun, W.: The near-field characteristics of circular jets at low Reynolds numbers. Mech. Res. Commun. **23**, 313–324 (1996)
3. Boguslawski, L., Popiel, C.O.: Flow structure of the free round turbulent jet in the initial region. J. Fluid Mech. **90**, 531–539 (1979)
4. Burattini, P., Antonia, R.A., Rajagopalan, S., Stephens, M.: Effect of initial conditions on the near-field development of a round jet. Exp. Fluids **37**, 56–64 (2004)
5. Burattini, P., Djenidi, L.: Velocity and passive scalar characteristics round jet with grids at the nozzle exit. Flow Turbulence Combust. **72**, 199–218 (2004)
6. Cohen, J., Wygnanski, I.: The evolution of instabilities in the axisymmetric jet. part 1. The linear growth of disturbances near the nozzle. J. Fluid Mech. **176**, 191–219 (1987)
7. Crow, S.C., Champagne, F.H.: Orderly structure in jet turbulence. J. Fluid Mech. **48**, 547–591 (1971)
8. Dimotakis, P.E., Miake-Lye, R.C., Papantoniou, D.A.: Structure and dynamics of round turbulent jets. Phys. Fluids **23**, 3185–3192 (1983)
9. Drubka, R., Reisenthel, P., Nagib, H.: The dynamics of low initial disturbance turbulent jets. Phys. Fluids A **1**, 1723–1735 (1989)
10. Eckmann, J.P.: Roads to turbulence in dissipative dynamical systems. Rev. Mod. Phys. **53**, 643–654 (1981)
11. Ferdman, E., Otugen, M., Kim, S.: Effect of initial velocity profiles on round jets. J. Propuls. Power **16**, 676–686 (2000)
12. George, W.K.: Recent advances in Turbulence, chapter the self-preservation of turbulent flows and its relation to initial conditions and coherent structures, pp. 39–73. Hemisphere, New York (1989)
13. Grandchamp, X.: Modélisation Physique des Écoulements Turbulents Appliquée aux voies Aériennes Supérieures Chez l'humain. PhD thesis, Grenoble University (2009)
14. Grandchamp, X., Van Hirtum, A., Pelorson, X.: Hot film/wire calibration for low to moderate flow velocities. Meas. Sci. Technol. **21**, 115402 (2010)
15. Grinstein, F.F., Glauser, M.N., George, W.K.: Fluid vortices. In: chapter Vorticity in jets, pp. 65–94. Kluwer Academic Publisher, New York (1995)
16. Harsha, P.T.: Free turbulent mixing: a critical evaluation of theory and experiment. Technical report (1971)
17. Ho, C., Huerre, P.: Perturbed free shear layers. Annu. Rev. Fluid Mech. **16**, 365–424 (1984)
18. Hussain, A., Zedan, M.: Effects of the initial condition on the axisymmetric free shear layer: effects of the initial momentum thickness. Phys. Fluids **20**, 1100–1112 (1978)
19. Hussein, H., Capp, S., George, W.: Velocity measurements in a high Reynolds number momentum conserving axisymmetric turbulent jet. J. Fluid Mech. **258**, 31–75 (1994)
20. Iyogun, C.O., Birouk, M.: Effect of sudden expansion on entrainment and spreading rates of a jet issuing from asymmetric nozzles. Flow Turbul. Combust. **82**, 287–315 (2009)

21. Kwon, S.J., Seo, I.W.: Reynolds number effects on the behavior of a non-buoyant round jet. Exp. Fluids **38**, 801–812 (2005)
22. Lee, S.S., Liu, J.T.C.: Multiple lare-scale coherent mode interactions in a developing round jet. J. Fluid Mech. **248**, 383–401 (1993)
23. Liepmann, D., Gharib, M.: The role of streamwise vorticity in the near-field entrainment of round jets. J. Fluid Mech. **245**, 643–668 (1992)
24. Malmström, T.G., Kirkpatrick, A.T., Christensen, B., Knappmiller, K.D.: Centreline velocity decay measurements in low-velocity axisymmetric jets. J. Fluid Mech. **246**, 363–377 (1997)
25. Mi, J., Kalt, P., Nathan, G., Wong, C.: PIV measurements of a turbulent jet issuing from round sharp-edged plate. Exp. Fluids **42**(2), 625–637 (2007)
26. Mi, J., Nathan, G., Luxton, R.: Centreline mixing characteristics of jets from nine differently shaped nozzles. Exp. Fluids **28**(2), 93–94 (2000)
27. Mi, J., Nobes, D., Nathan, G.: Influence of jet exit conditions on the passive scalar field of an axisymmetric free jet. J. Fluid Mech. **432**, 91–125 (2001)
28. Michalke, A. On spatially growing disturbances in an inviscid shear layer. J. Fluid Mech. **23**, 521–544 (1965)
29. Michalke, A., Hermann, G.: On the inviscid instability of a circular jet with external flow. J. Fluid Mech. **114**, 343–359 (1982)
30. Mikhail, M.N.: Optimum design of wind tunnel contractions. AIAA J. **17**, 471–477 (1979)
31. Morel, T.: Comprehensive design of axisymmetric wind tunnel contractions. J. Fluid Eng. **97**, 225–233 (1975)
32. Panchapakesan, N., Lumley, J.: Turbulence measurements in axisymmetric jets of air and helium. Part 1. Air jet. J. Fluid Mech. **246**, 197–224 (1993)
33. Pitts, W.: Reynolds number effects on the mixing behavior of axisymmetric turbulent jets. Exp. Fluids **11**, 135–141 (1991)
34. Quinn, W.: Upstream nozzle shaping effects on near field flow in round turbulent free jets. Eur. J. Mech. B, Fluids **25**, 279–301 (2006)
35. Romano, G., Antonia, R.A.: Longitudinal and transverse structure functions in a turbulent round jet: effect of initial conditions and Reynolds number. J. Fluid Mech. **436**, 231–248 (2001)
36. Russ, S., Strykowski, P.: Turbulent structure and entrainment in heated jets: The effect of initial conditions. Phys. Fluids **5**, 3216–3225 (1993)
37. Saffman, P.G.: Vortex dynamics. Cambridge Monographs on Mechanics and Applied Mathematics, pp. 1–311. New York (2001)
38. Sautet, J., Stepowski, D.: Dynamic behavior of variable-density, turbulent jets in their near development fields. Phys. Fluids **7**(2), 2796–2806 (1995)
39. Schlichting, H., Gersten, K.: Boundary Layer Theory. Springer Verlag, Berlin (2000)
40. Todde, V., Spazzini, P.G., Sandberg, M.: Experimental analysis of low-Reynolds number free jets: evolution along the jet centerline and Reynolds number effects. Exp. Fluids **47**, 279–294 (2009)
41. Van Hirtum, A., Grandchamp, X., Pelorson, X.: Moderate Reynolds number axisymmetric jet development downstream an extended conical diffuser: influence of extension length. Eur. J. Mech. B, Fluids **28**, 753–760 (2009)
42. Winant, C.D., Browand, F.K.: Vortex pairing: the mechanism of turbulent mixing-layer growth at moderate Reynolds number. J. Fluid Mech. **63**, 237–255 (1974)
43. Wygnanski, I., Sokolov, M., Friedman, D.: On transition in a pipe: Part 2. The equilibrium puff. J. Fluid Mech. **69**, 283–304 (1975)
44. Wygnanski, I.J., Champagne, F.H.: On transition in a pipe: Part 1. The origin of puffs and slugs and the flow in a turbulent slug. J. Fluid Mech. **59**, 281–335 (1973)
45. Xu, G., Antonia, R.A.: Effect of different initial conditions on a turbulent round free jet. Exp. Fluids **33**, 677–683 (2002)
46. Zaouali, Y., Filali, T., Ben, H., Aissia, Jay, J.: Flow structure generated from an axisymmetric natural air jet at a moderate reynolds number. Fluid Dyn. Res. **43**, 1–13 (2011)